Bimetallic oxide $Cu_2O@MnO_2$ with exposed phase interfaces for dual-effect purification of indoor formaldehyde and pathogenic bacterium

Jia Yu Zheng[†,1], Hao Zhang[†,1], Jun Da He[†,2], Bo Hai Tian[1], Chang Bao Han[*,1], Zhixiang Cui[*,3], Hui Yan[1]

[1] The Key Laboratory of Advanced Functional Materials, Ministry of Education of China, Faculty of Materials and Manufacturing, Beijing University of Technology, Beijing 100124, People's Republic of China

[2] Key laboratory of Beijing on Regional Air Pollution Control, Beijing University of Technology, Beijing 100124, People's Republic of China

[3] College of Materials Science and Engineering, Fujian University of Technology, Fujian, Fuzhou, 350118, People's Republic of China

[†] The authors contribute equally to the article

[*] Corresponding author. E-mail: cbhan@bjut.edu.cn, cuizhixiang2006@126.com

Supporting Information (I)

Theoretical calculation:

All the structural optimizations, energy calculations, and charge density difference analysis were carried out by DFT implemented in the Vienna Ab-initio Simulation Package (VASP) [1, 2]. The interaction between valence electrons and the ionic cores was calculated by the projector-augmented-wave (PAW) method [3, 4], and the related exchange-correlation energy was described by employed the Perdew-Burke-Ernzerhof approach of spin-polarized generalized gradient approximation (GGA-PBE) [5]. The cut-off plane-wave kinetic energy was set as 450 eV, and *k*-mesh grids were 4 × 2 × 1 for the integration of the Brillouin zone. The conjugate-gradient (CG) method with the total energy convergence criterion 10^{-5} eV was used to obtain the electronic relaxation [6]. Geometry optimization with the residual forces on unconstrained atoms less than 0.02 eV/Å was carried out by the quasi-Newton algorithm [7, 8]. To ensure the initial configuration correctly, an O_2 molecule was deposited on the catalyst surface and relaxed for calculating its local minimum total energy on different sites, and the lowest one is the initially stable configuration. The final configuration is also found by relaxing O near the O_2 absorbed site of the initial configuration. The O_2 and O absorbing on the slabs were investigated by comparing the formation energy of different sites. The equation for calculating the energy of oxygen activation ΔE_{O*} as the following:

$$\Delta E_{O*}=E_{slab+O*}-E_{slab+O2}$$

Where the $E_{slab+O*}$ is the total enthalpy of free radical O on the catalysts, $E_{slab+O2}$ is the total enthalpy of O_2 molecule adsorbing on the catalysts.

Supporting Information (II)

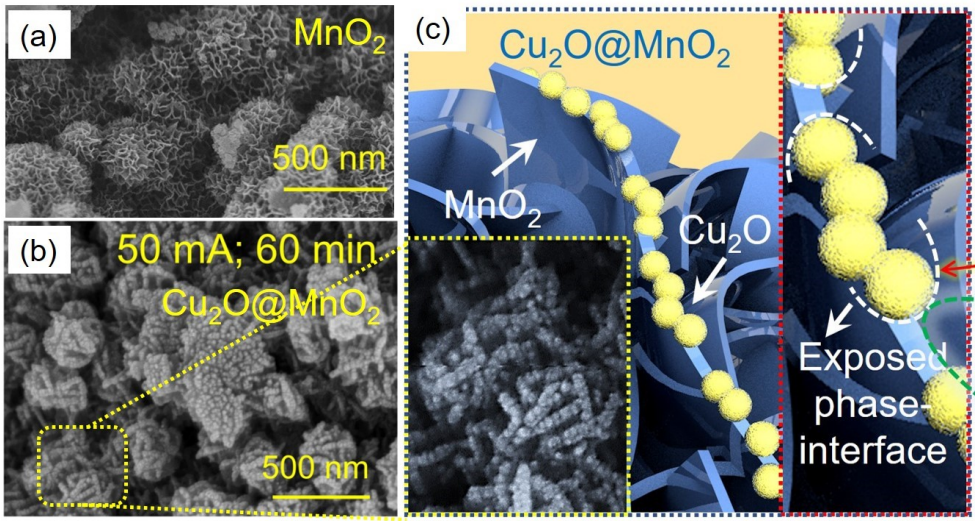

Fig. S1 SEM images of the (a) pure MnO_2 catalyst and (b) the bimetallic oxide $Cu_2O@MnO_2$. (c) The diagram of phase-interface in $Cu_2O@MnO_2$.

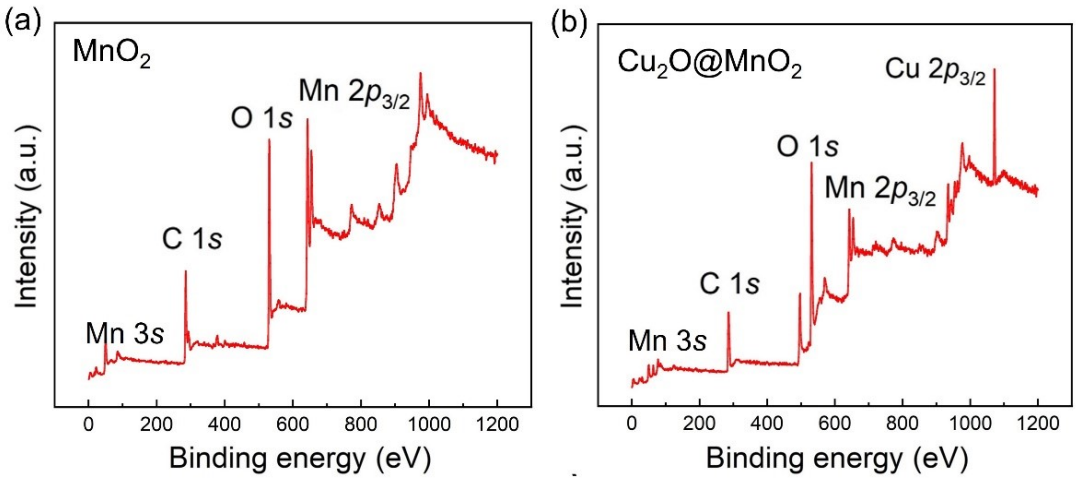

Fig. S2 XPS survey spectrum of the sample of (a) MnO_2 and (b) $Cu_2O@MnO_2$.

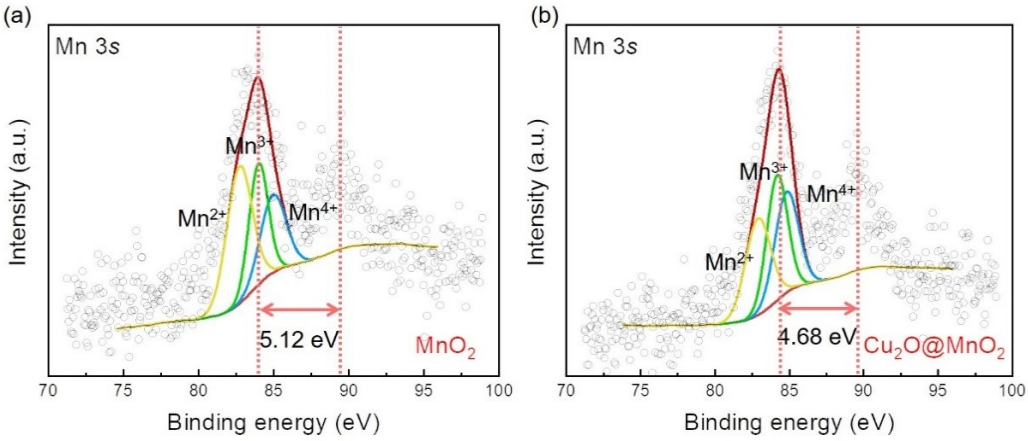

Fig. S3 The XPS spectrum of (a) MnO_2 and (b) $Cu_2O@MnO_2$ in Mn3*s*.

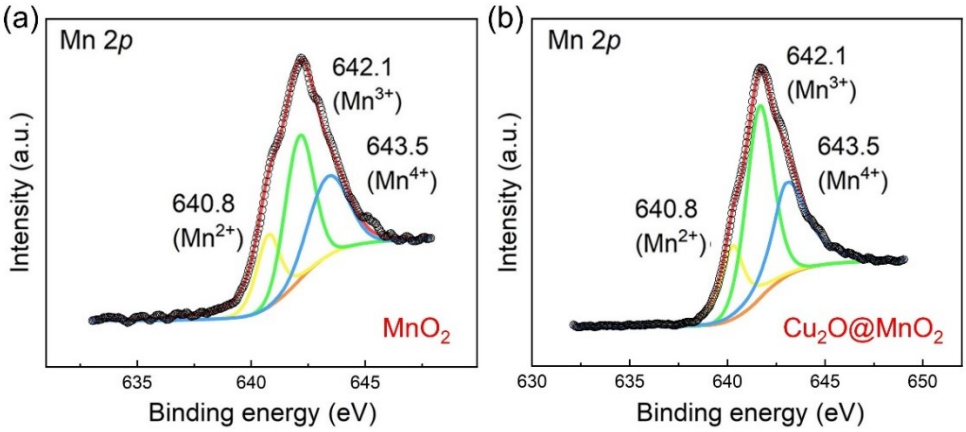

Fig. S4 The XPS spectrum of (a) MnO_2 and (b) $Cu_2O@MnO_2$ in Mn2*p*.

Table S1. Ratio of peak area in different elements determined by the fitting result of XPS.

Sample	Ratio of peak area									
	Mn 3*s*			Mn 2*p*			O 1*s*			Cu 2*p*
	Mn (II)	Mn (III)	Mn (IV)	Mn (II)	Mn (III)	Mn (IV)	$O_{lattice}$	$O_{adsorbed}$ -OH	O_{H2O}	Cu-O
MnO_2	35%	32%	33%	18%	39%	43%	52%	29%	19%	-
$Cu_2O@MnO_2$	31%	33%	36%	16%	53%	31%	29%	47%	24%	-

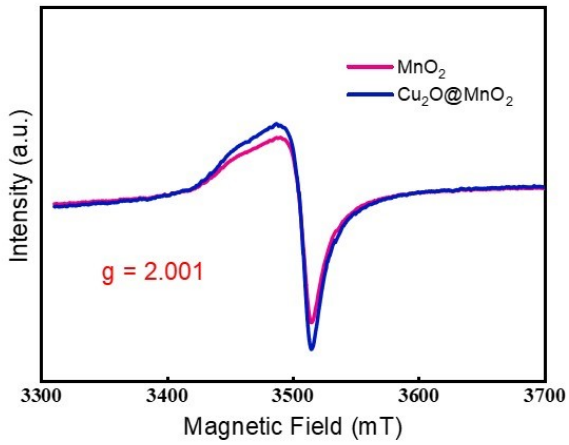

Fig. S5 EPR spectra of the samples of MnO_2 and $Cu_2O@MnO_2$.

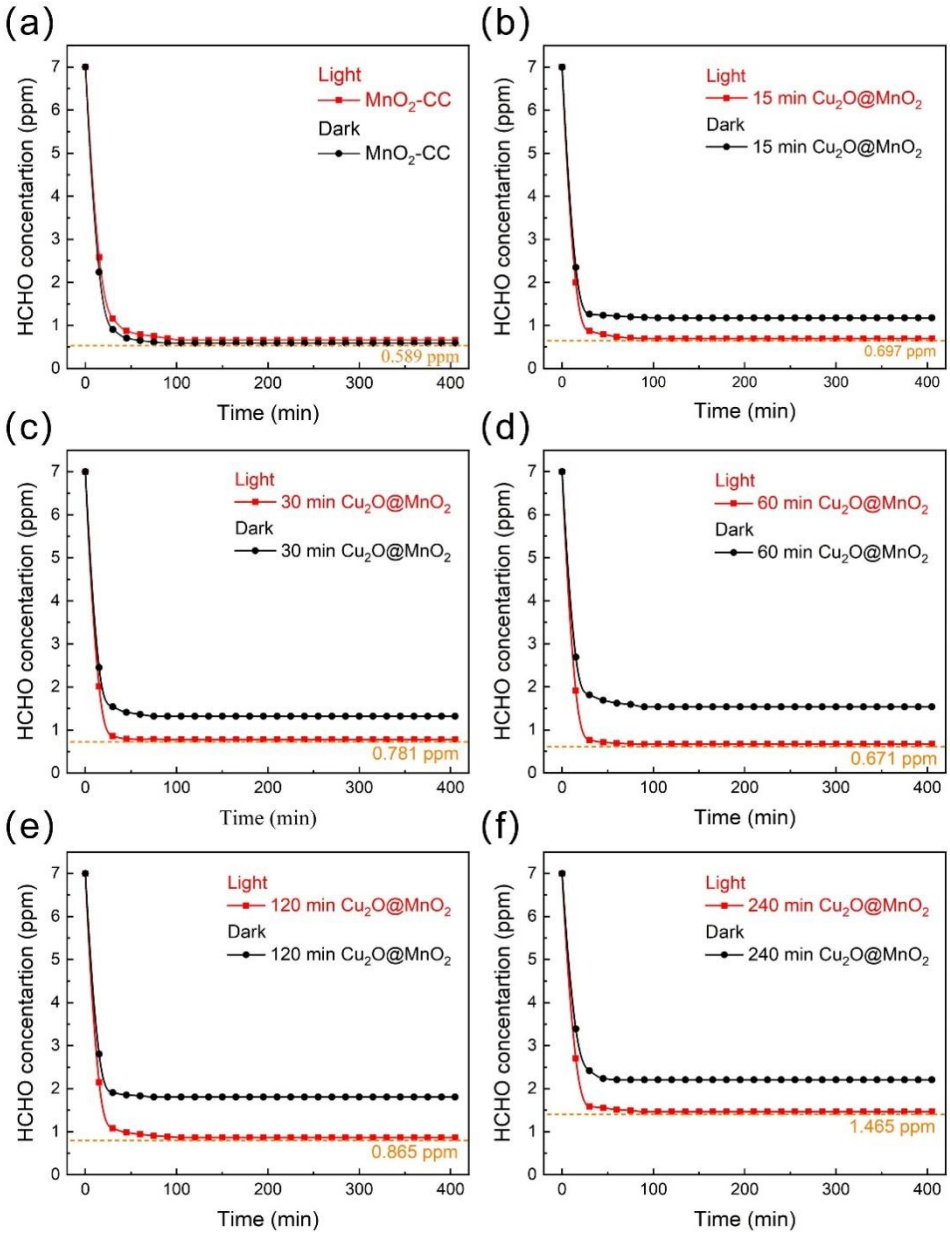

Fig. S6 Comparison of HCHO removal efficiency between MnO_2-CC and $Cu_2O@MnO_2$ under light and dark conditions, (a) MnO_2-CC, (b) 15 min $Cu_2O@MnO_2$, (c) 30 min $Cu_2O@MnO_2$, (d) 60 min $Cu_2O@MnO_2$, (e) 120 min $Cu_2O@MnO_2$, (f) 240 min $Cu_2O@MnO_2$

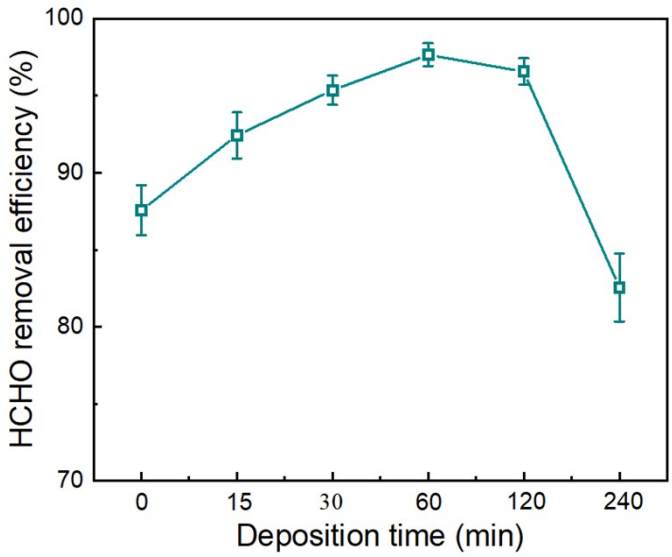

Fig. S7 Dynamic HCHO removal efficiency of $Cu_2O@MnO_2$ with different deposition times as a function of reaction time

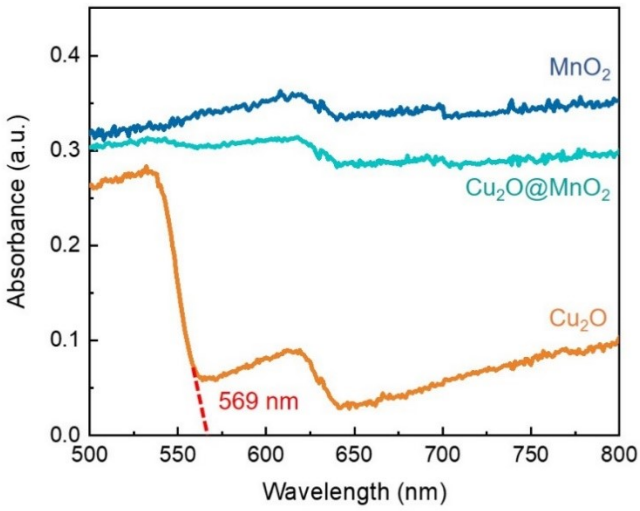

Fig. S8 UV-VIS-NIR diffuse-reflectance spectra testing of different samples Cu_2O, $Cu_2O@MnO_2$ and MnO_2.

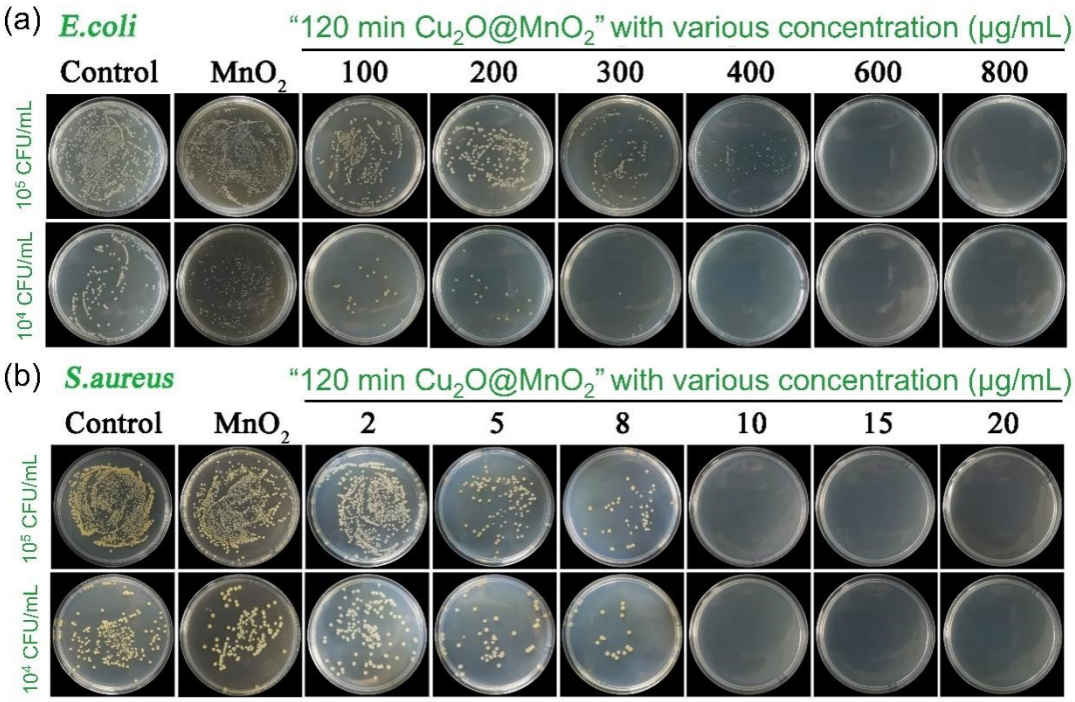

Fig. S9 The photos of MIC experimental colony growth against different pathogenic bacteria under the action of the bimetallic oxide sample $Cu_2O@MnO_2$

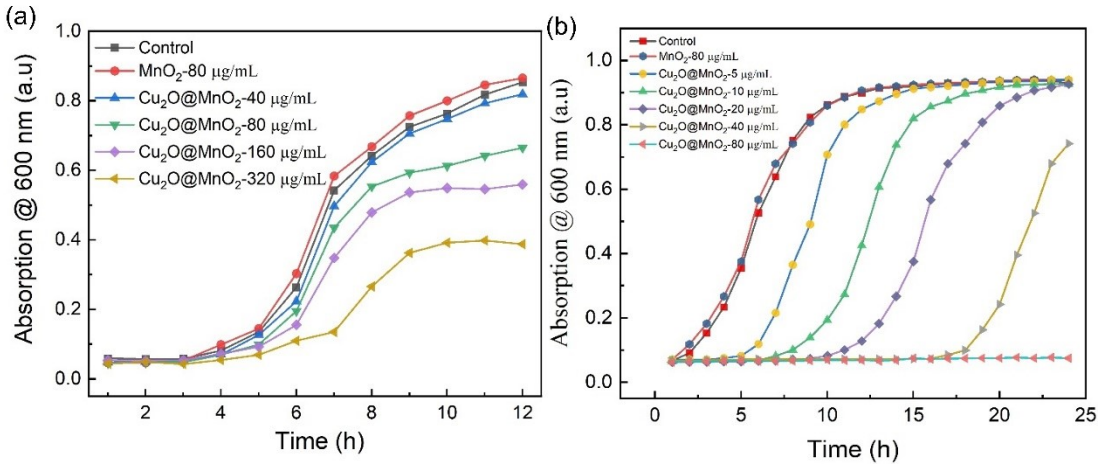

Figure S10 Growth inhibition curves of *E.coli* and *S. aureus* with different concentrations of the bimetallic oxide sample $Cu_2O@MnO_2$

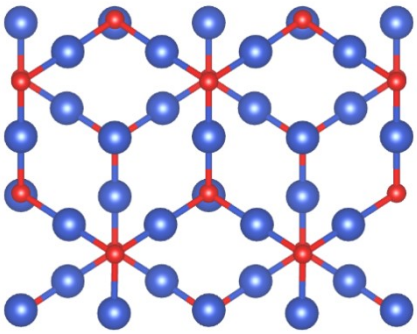

Figure S11 Theoretical calculation model of Cu_2O.

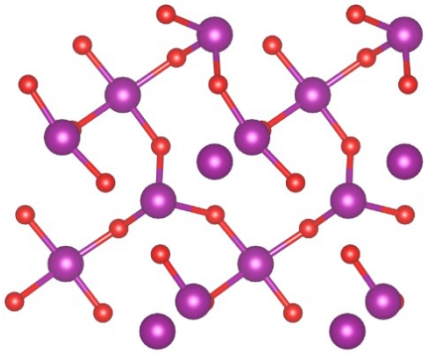

Figure S12 Theoretical calculation model of MnO_2.

Reference

[1] G. Kresse, J. Furthmüller, J. Hafner, Theory of the crystal structures of selenium and tellurium: The effect of generalized-gradient corrections to the local-density approximation, Phys. Rev. B, 50 (1994) 13181.

[2] G. Kresse, J. Furthmiiller, Efficiency of ab-initio total energy calculations for metals and semiconductors using a plane-wave basis set, Comp. Mater. Sci., 6 (1996) 15-50.

[3] P.E. Blöchl, Projector augmented-wave method, Phys. Rev. B, 50 (1994) 17953.

[4] G. Kresse, D. Joubert, From ultrasoft pseudopotentials to the projector augmented-wave method, Phys. Rev. B, 59 (1999) 1758-1775.

[5] J.P. Perdew, K. Burke, M. Ernzerhof, Generalized Gradient Approximation Made Simple, Phys. Rev. Lett., 78 (1997) 1396.

[6] M.C. Payne, M.P. Teter, D.C. Allan, T.A. Arias, J.D. Joannopoulos, Iterative minimization techniques for ab initio total-energy calculations: molecular dynamics and conjugate gradients, Rev. Mod. Phys., 64 (1992) 1045.

[7] PéterPulay, Convergence acceleration of iterative sequences. the case of scf iteration, Chemical Physics Letters, 73 (1980) 393-398.

[8] M. Methfessel, A.T. Paxton, High-precision sampling for Brillouin-zone integration in metals, Phys. Rev. B, 40 (1989) 3616.